Near-Unity Internal Quantum Efficiency of Luminescent Silicon Nanocrystals with Ligand Passivation

Fatemeh Sangghaleh,[†] Ilya Sychugov,[*,†] Zhenyu Yang,[‡] Jonathan G. C. Veinot,[‡] and Jan Linnros[†]

[†]Materials and Nano Physics Department, ICT School, KTH-Royal Institute of Technology, 16440 Kista, Sweden and [‡]Department of Chemistry, University of Alberta, Edmonton, Alberta T6G 2G2, Canada

ABSTRACT Spectrally resolved photoluminescence (PL) decays were measured for samples of colloidal, ligand-passivated silicon nanocrystals. These samples have PL emission energies with peak positions in the range ~1.4−1.8 eV and quantum yields of ~30−70%. Their ensemble PL decays are characterized by a stretched-exponential decay with a dispersion factor of ~0.8, which changes to an almost monoexponential character at fixed detection energies. The dispersion factors and decay rates for various detection energies were extracted from spectrally resolved curves using a mathematical approach that excluded the effect of homogeneous line width broadening. Since nonradiative recombination would introduce a random lifetime variation, leading to a stretched-exponential decay for an ensemble, we conclude that the observed monoexponential decay in size-selected ensembles signifies negligible nonradiative transitions of a similar strength to the radiative one. This conjecture is further supported as extracted decay rates agree with radiative rates reported in the literature, suggesting 100% internal quantum efficiency over a broad range of emission wavelengths. The apparent differences in the quantum yields can then be explained by a varying fraction of "dark" or blinking nanocrystals.

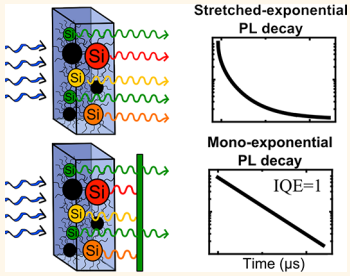

KEYWORDS: photoluminescence decay · radiative rate · nonradiative channel · lifetime · dispersion factor

Silicon nanocrystals (Si NCs), which initially attracted attention due to their possible optoelectronics applications,[1−3] are ideal candidates for biomedical imaging and diagnostic applications because of their established nontoxicity, biocompatibility, and material abundance.[4−6] Despite the indirect band gap of bulk silicon, strong visible luminescence is observed when reduced to nanometer size scale, originally discovered in porous silicon over 20 years ago.[7,8] Throughout the ensuing decades various optical properties of Si NCs have been extensively studied,[9,10] including the ensemble photoluminescence (PL) absolute quantum yield (QY).[11,12] Reported QY values differ from several percent for Si NCs embedded in SiO_2[13,14] to about 60% for colloidal NCs.[15,16] The QY, which is also referred to as the external quantum efficiency, is defined as the ratio of emitted to absorbed photons by an ensemble of NCs and therefore includes all possible processes inside the Si NC assembly. To gain a better insight into the recombination mechanism, the internal quantum efficiency, IQE = $\Gamma_r/(\Gamma_r + \Gamma_{nr})$, should also be determined, where Γ_r and Γ_{nr} are the PL radiative and nonradiative decay rates, respectively. Unlike QY, this parameter describes the efficiency for only "bright" nanocrystals and represents only the ON-state efficiency for blinking nanoparticles. "Dark" nanocrystals, characterized by very efficient nonradiative recombination (*e.g.*, due to the presence of defects), as well as blinking nanocrystals in their OFF-state,[17] still contribute to absorption and accordingly lower the QY. Thus, mathematically we can express QY in terms of the IQE of individual NCs and the blinking duty cycle δ (fraction of time in ON-state) as QY = $(\sum_{i=1}^{N_{BR}} \delta_i \mathrm{IQE}_i)/(N_{BR} + N_{Dark})$, where N_{BR} and N_{Dark} are the number of bright and dark NCs, respectively.

Skryshevsky *et al.*[18] reported an IQE ≈ 8% for porous silicon, almost double the total QY, by measuring current changes in a p−n junction due to porous silicon photoemission. Recently, we obtained a similar value of IQE ≈ 9% for isolated single Si nanoparticles prepared by lithography and oxidation.[19] By a different approach, based on the effect of photonic mode density on the

* Address correspondence to ilyas@kth.se.

Received for review March 20, 2015 and accepted June 17, 2015.

Published online June 17, 2015
10.1021/acsnano.5b01717

radiative recombination rate, Walters *et al.*[20] and Kalkman *et al.*[21] extracted Γ_r and estimated ~40−80% IQE for Si NCs embedded in SiO_2 prepared by ion implantation and annealing. The exact wavelength dependence of Γ_r measured by this technique revealed IQEs approaching even 100% for large nanoparticles emitting in a limited energy range (1.4−1.5 eV).[22] From this we conclude that the IQE is very sample-dependent for Si NC/SiO_2 systems, suggesting the presence of a nonradiative process with a similar strength to the radiative one, where the exact interplay between these two in a given sample defines the IQE. A possible source of this nonradiative process is an interfacial state between Si and SiO_2[22,23] or a defect in the oxide shell.[24]

RESULTS AND DISCUSSION

In this work, we present PL measurements of fully radiative, ligand-passivated Si NCs covering a broad range of emission energies (1.2−2.2 eV). These are colloidal nanocrystal dispersions derived from a silicon/oxygen compound, thus different from nanocrystals in an oxide matrix as discussed above. To find the IQE, spectrally resolved PL decays (spectral resolution $\Delta\lambda \approx 3$ nm) of Si NC ensembles were studied. The intrinsic PL decay times τ_{0i} and dispersion factors β_i of the stretched-exponential transients were extracted for various detection energies (E_{det}) taking into account the homogeneous line width broadening effect. A transition from stretched-exponential to monoexponential decay curve was confirmed for spectrally selected luminescence. Furthermore, we have found that the decay time decreases monotonically with increasing energy (smaller NC size), as expected from quantum confinement theory,[25] and coincides with radiative rates reported from other studies,[22] which indicates 100% IQE in the studied Si NC dispersions.

Oxide-embedded Si NCs were synthesized by annealing dried commercial hydrogen silsesquioxane solution at 1100 °C in a slightly reducing atmosphere with 5% H_2. Hydride-terminated NCs were freed from the oxide matrix using a well-established HF etching protocol, functionalized with different ligands, and purified prior to analysis.[26] Compared to the other techniques that afford spherical and pseudospherical NCs,[27,28] size and morphology can be controlled more precisely using the chosen method *via* rational variation of the processing time and temperature.[29] Fourteen various samples of Si NCs prepared with different surface ligands using different passivation procedures were evaluated optically. The NCs with highest and lowest luminescence peak energy positions and decay rates (samples A and F, respectively), as well as four with intermediate emission energies and decay times (samples B, C, D, and E), were selected for a detailed study. These samples were labeled in alphabetic order for clarity, as summarized in Table 1. Among these samples B, C, and D were dodecyl-passivated, while samples E and F were passivated by methyl undecanoate, and sample A was passivated by hexyl groups. All samples except B and D were functionalized using radical-assisted hydrosilylation using azobis(isobutyronitrile) (AIBN)[30] as a radical initiator, while sample B was functionalized using photochemically initiated hydrosilylation,[31] and sample D by thermal initiation.[26]

TABLE 1. Overview of the Samples Prepared *via* Different Preparation Parameters, Labeled in Alphabetic Order

sample code	nominal label	nominal NC size	surface ligands	passivation method
A	INI-1P	3 nm	hexyl	radical initiated
B	1100-34	3 nm	dodecyl	photochemical
C	StySi-14P	3 nm	dodecyl	radical initiated
D	1100-30	3 nm	dodecyl	thermal initiated
E	INI-30	5 nm	methyl undecanoate	radical initiated
F	INI-29	5 nm	methyl undecanoate	radical initiated

Figure 1a shows PL emission spectra and relative absorption of selected ligand-passivated Si NCs. The two samples with highest and lowest PL peak positions (A and F) have correspondingly different absorption edge onsets as well, with a typical relation of the band-gap energy with the absorption onset for Si NC ensembles.[9] The size distribution and uniformity of these NCs were verified by transmission electron microscopy (TEM) imaging, as shown in Figure 1b, with associated particle size histograms in Figure 1c.

The results presented in Figure 1 indicate a shift toward higher energies with decreased Si NC diameter consistent with quantum confinement. Absolute quantum yields of 14 samples of Si NCs as a function of their emission peak position are shown in Figure 2, left. The randomly distributed QYs of ~30−70% reveal that the total luminescence efficiency is influenced by many parameters (*e.g.*, surface/interface defects introduced by passivation/preparation methods) rather than only NC size (emission energy). A detailed study on the effect of surface passivation on QYs of such Si NCs is a subject of a separate study, and here we focus on the IQE of such nanoparticles. Figure 2, right, presents PL decay times and dispersion factors of Si NCs passivated with different ligands. Consistent with previous reports for ensembles of Si NCs,[32] the PL decays take the form of a "stretched-exponential", $I = I_0 \exp(-(t/\tau)^{\beta})$ where τ and β are the lifetime and dispersion factor, respectively (inset in Figure 2). In contrast to fast decays (ns or ps) of emission of Si NCs reported in the literature, which was ascribed to molecular-like structures,[33] defect sites,[34] or hot exciton recombination,[35] here ensemble PL decays are in the microsecond range, corresponding to quantum-confined transitions.[36] Recently we demonstrated that a single nanocrystal

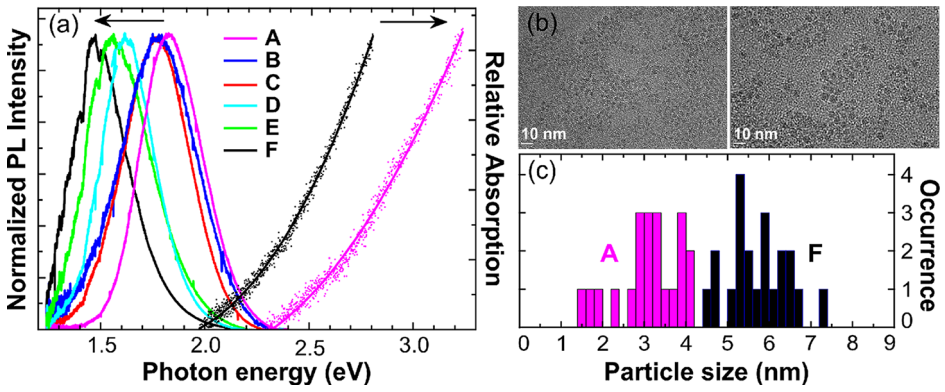

Figure 1. (a) PL emission spectra of various ligand-passivated Si NCs at room temperature (PL line width and peak position are independent of the excitation wavelength). Relative PL absorption of Si NCs with maximum and minimum luminescence energy peak positions (samples A and F) is shown in the same plot. (b) Bright-field TEM images of Si NCs drop-cast onto amorphous SiN membranes (A to the left and F to the right) with (c) histograms showing corresponding average size distributions of ~3 and 5.5 nm, respectively.

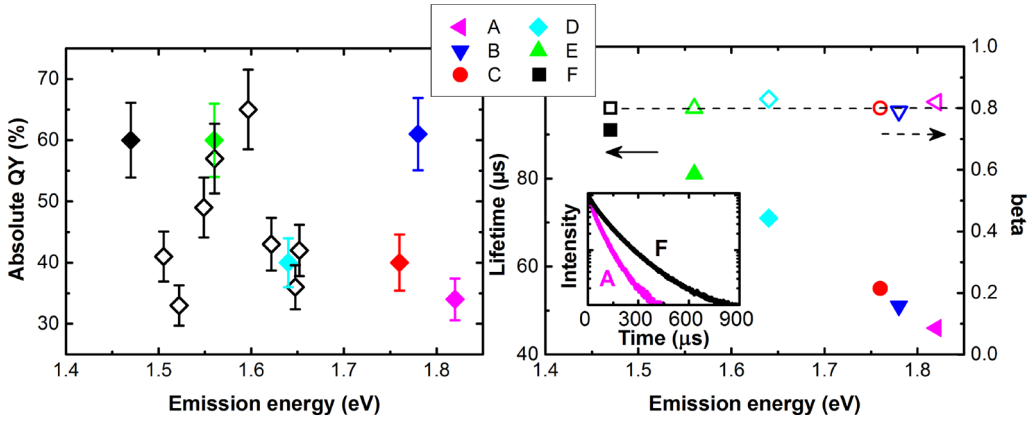

Figure 2. (Left) Absolute PL quantum yields of 14 samples of Si NCs with different ligands and passivation procedure *versus* their emission energies. Error bars represent the uncertainty due to the system response calibration and low absorption in the samples. (Right) PL decay times (solid symbols) and dispersion factors β (empty symbols), as a function of emission energy, extracted from a stretched-exponential fit to the PL decay data. Examples of stretched-exponential decays for samples A and F are shown in the inset.

exhibits a monoexponential decay in the microsecond range;[37] from this we conclude the stretched-exponent of the ensemble can be interpreted as a linear combination of individual decay curves. In this context, the dispersion factor β ($0 < \beta < 1$) represents the measure of individual rate variation in the sample (the smaller the β, the larger the dispersion).[36] Here the ensemble PL decay times were in the range 45 to 90 μs, and the dispersion factor is ~0.8 for all the samples as seen from Figure 2, right. Note that these PL decay times are longer than those we previously reported (5−45 μs) for single Si dots with a thick oxide shell[37] where the IQE is ~9% due to the low oxidation temperature used (900 °C).[19]

The results of the standard optical and structural characterization of ligand-passivated Si NCs discussed above are typical for this material system.[38] We now turn the discussion to the determination of IQE in the present samples using spectrally resolved PL decay measurements. Figure 3 shows PL decay curves of sample F, normalized to the corresponding measured lifetime τ_{0m}, obtained for the whole ensemble (black) and detected at E_{det} = 1.82 eV and E_{det} = 1.51 eV (blue and green, respectively). From Figure 3 it is clear that the measured dispersion factor β_m is larger (between ~0.85 and 1) in the case of spectrally selected detection, and the actual β_m value depends on energy (solid black triangles in Figure 3, inset), deviating more from unity at larger detection energies (E_{det}). The same trend and absolute values were observed for sample A (Figure S1) as well as for Si NCs embedded in SiO_2,[36] while the absolute values are lower (open triangles in the inset of Figure 3). Considering that the homogeneous line width of the PL from ligand-passivated Si NCs is quite broad at room temperature (~200 meV),[39] the NCs with the emission energies close to the detection energy contribute to the measured signal as well and influence the measured decay parameters τ_{0m} and β_m for a given E_{det}. From Figure 2b one can note that NCs with larger emission energies have shorter lifetimes. Thus, the deviation of β_m from unity at larger emission energies can be intuitively understood

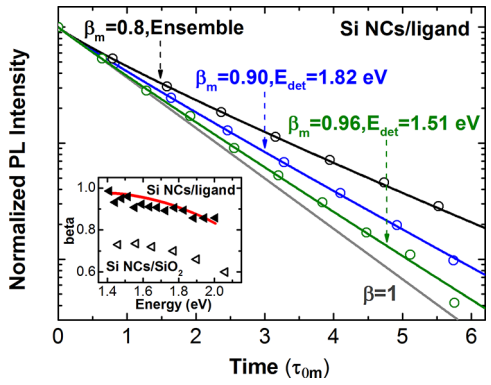

Figure 3. PL decays (open symbols) and related stretched-exponential fit (solid lines) of sample F, normalized to corresponding lifetime values (τ_{0m}), for the full ensemble of Si NCs (black), and at detection energies of 1.82 and 1.51 eV (blue and green, respectively). A monoexponential function is also plotted for reference (gray line). The dispersion factor β_m is clearly larger for the spectrally selected decays. The inset shows β_m extracted for different detection energies (filled black triangles) and β_{sim} simulated (without any fitting parameters) considering the effect of homogeneous broadening (red solid line). β_m values of Si NCs implanted in SiO_2[36] are also shown (open triangles) for comparison.

considering that for shorter lifetimes the relative variation in contributed lifetime $\tau_{0i}(\varepsilon)$ values from neighboring color nanocrystals is larger, resulting in a stronger dispersion (*i.e.*, lower β). On the other end of the detection energy range, relative variations in $\tau_{0i}(\varepsilon)$ values are small and β maintains its close to unity intrinsic value, being only little affected by contributions from spectrally adjacent nanocrystals. The exact effect of this contribution has been evaluated numerically using a known ensemble emission spectrum, lifetime energy dependence, and homogeneous line width values as described below.

The measured ensemble emission spectrum can be very well fitted by a Gaussian function (*e.g.*, with adjusted *R*-square = 0.987 for sample F, Figure 1a) and represents the distribution of nanocrystals with different emission energy ε:

$$I_{ens}(\varepsilon) \approx \exp\left(-2\frac{(\varepsilon - E_0)^2}{\omega_{ens}^2}\right) \quad (1)$$

where ω_{ens} is the width of the ensemble distribution ($\omega_{ens} \approx 270$ meV, *cf.* Figure 1a) and E_0 is its peak position. Then the intensity of nanocrystals with different emission energy ε that contribute to the detected signal at energy E_{det} is given by

$$I_{det}(\varepsilon) = I_{ens}(\varepsilon)\exp\left(-2\frac{(E_{det} - \varepsilon)^2}{\omega_{hom}^2}\right) \quad (2)$$

where ω_{hom} is a homogeneous peak width ($\omega_{hom} \approx 200$ meV).[39] Finally, the measured decay curve as a function of time for a given detection energy $I_{det}(t) \approx \exp(-(t/\tau_{0m})^{\beta m})$ is a combination of individual decays, $\sim\exp(-t/\tau_{0i}(\varepsilon))$, of all contributing nanocrystals with emission energy ε and intrinsic lifetime $\tau_{0i}(\varepsilon)$:

$$I_{det}(t) = \int I_{det}(\varepsilon)\exp\left(-\frac{t}{\tau_{0i}(\varepsilon)}\right)d\varepsilon \quad (3)$$

where integration, in general, should be taken over the whole emission spectrum. Collecting eqs 1−3 we get the following expression:

$$I_{det}(t) \approx \int \exp\left(-2\left(\frac{(\varepsilon - E_0)^2}{\omega_{ens}^2} + \frac{(E_{det} - \varepsilon)^2}{\omega_{hom}^2}\right)\right) \times \exp\left(-\frac{t}{\tau_{0i}(\varepsilon)}\right)d\varepsilon \quad (4)$$

Thus, it is possible to numerically construct a decay curve for a given detection energy using experimentally obtained luminescence parameters E_0, ω_{ens}, and ω_{hom} and known $\tau_{0i}(\varepsilon)$.

In practice when a decay time (τ_{0m}) is measured, the homogeneous line width effect is already included in the data. Thus, in order to extract intrinsic lifetime $\tau_{0i}(\varepsilon)$ values, it is necessary to solve an inverse problem. We carried out this procedure by assuming an intrinsic lifetime $\tau_{0i}(\varepsilon)$ close to the measured one $\tau_{0m}(\varepsilon)$ and then comparing the simulated decay lifetimes to the measured ones. This procedure was repeated in several iterations until the assumed intrinsic $\tau_{0i}(\varepsilon)$ led to the measured decay lifetimes $\tau_{0m}(\varepsilon)$ as an effect of homogeneous broadening. Then we have simulated the exact shape of decay curves at different E_{det} according to eq 4 and obtained dispersion factors $\beta_{sim}(E_{det})$. The simulated dispersion factors β_{sim} are shown as a function of the detection energy as a red line in the inset of Figure 3. As seen from Figure 3, the β_{sim} values exhibit the same energy dependence with nearly identical absolute values as the experimentally obtained β_m. Note that there were no fitting parameters used in the simulation procedure. Thus, the only reason for the observed deviation of β_m from unity is the homogeneous broadening, and we have successfully reproduced our data using a strict emission energy−size correlation with intrinsic $\beta_i(E_{det}) = 1$. In this way by excluding the homogeneous line width broadening contribution into the measured decay signal a size selection method has been applied here mathematically without physical size separation of nanocrystals. In fact, through the introduced numerical method, the spectrally resolved decays of Si NCs were mathematically converted to size-selected decays. Therefore, the expression of "size-selected Si NCs" used in the article is referred to the mathematical exclusion of the homogeneous line width broadening in spectrally resolved measurements.

The lack of lifetime dispersion in size-selected ensembles of ligand-passivated Si NCs is an important result, indicating that there is no room for a random lifetime variation for a given energy, as would be the case for an appreciable nonradiative recombination

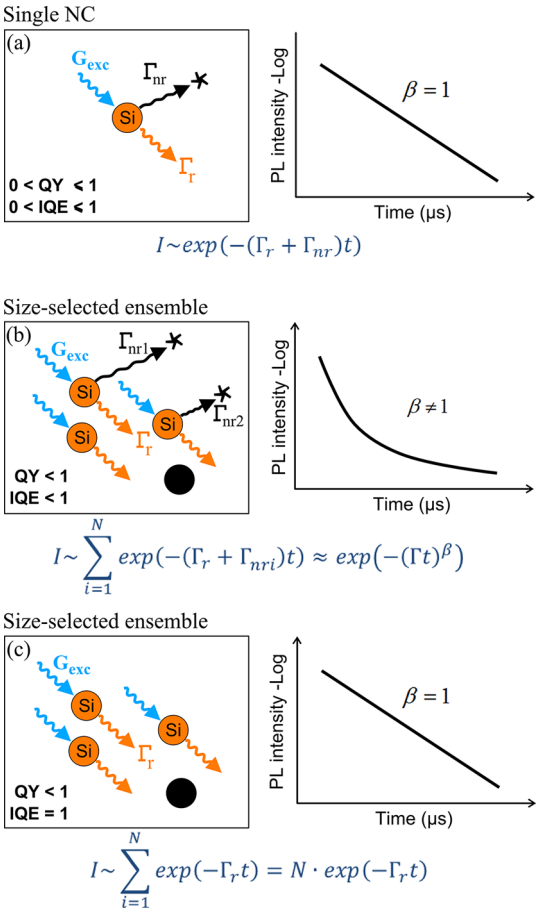

Figure 4. Schematic of the impact of various PL recombination channels on the shape of the PL decay curve of a (a) single and (b) size-selected ensemble of Si NCs with IQE < 1 and with (c) IQE = 1. The star-like symbols illustrate adjacent to NCs defect sites, considered as the likely origin of a microsecond nonradiative process. Dark NCs are shown as black circles. G_{exc}, Γ_r, and Γ_{nr} are excitation, radiative, and nonradiative decay rates, respectively. Corresponding luminescence intensity decay formulas are also shown for each case.

effect (as indeed observed by single-dot measurements of oxide-passivated Si nanocrystals).[37] For clarity we have illustrated the impact of the PL lifetime variation on the decay curve shape for a single and for a size-selected ensemble of Si NCs in Figure 4. In general, in Si NC systems the nonradiative channels can be classified into three categories: (i) fast nonradiative transitions (*e.g.*, Auger process with a decay time of ~10 ns)[40] due to dangling bonds, defects, *etc.*,[41,42] which make nanocrystals dark; (ii) nonradiative channels with the decay rate similar to the radiative one,[37] which consequently affects IQE; and (iii) slow nonradiative transitions (*e.g.*, blinking with characteristic times of seconds or even minutes).[17] Dark circles and star-like symbols in Figure 4 are illustrations of type (i)/(iii) and type (ii) nonradiative channels, respectively. Figure 4a depicts the monoexponential characteristic of a single Si NC, which may contain various nonradiative transitions degrading the IQE. The decay here is monoexponential[37] for any IQE since the exciton has simultaneous access to all possible recombination pathways, and the total decay rate is the sum of various individual rates as shown in the formula below Figure 4a. For any subset of nanocrystals, however, the presence of two competing recombination channels (Figure 4b) will inevitably introduce dispersion in the total decay rate due to small structural variations in nanoparticles and hence varying access to these channels for e−h pairs in different nanocrystals (*e.g.*, $\Gamma_{nr1} \neq \Gamma_{nr2}$ or $\Gamma_{nr3} = 0$ as shown in Figure 4b). In that case the dispersion factor β would not reach unity for spectrally resolved ensemble decay curves since here the summation goes over individual decays with different total rates as expressed in the formula below Figure 4b. This situation corresponds to the case of Si NCs embedded in an oxide matrix, where the highest reported value for the measured dispersion factor in size-selected ensembles was only $\beta_m = 0.75$ (open triangles in the inset of Figure 3).[36] The absence of any competitive nonradiative channels in size-selected ensembles of Si NCs (Figure 4c) results in a near unity β as the outcome of the mathematical summation of individual monoexponential decays with the same PL lifetimes, which is the case observed in the current study (cf. Figure 3). Thus, the lack of dispersion in decay rates is conjectured here as a strong indication of 100% IQE considering the microscopic physical structure of defects (*cf.* Figure 4b and c). However, strictly speaking this is not a mathematically correct conjecture since for a hypothetical case of the same nonradiative channel for all nanoparticles with a given energy the decay curve would be monoexponential as well. To eliminate this possibility and to verify our conjecture independently, we compared the total intrinsic PL decay rates at various detection energies measured here (for samples A and F) with radiative decay rates measured for Si NCs from the literature.

Values of the total recombination rate $\Gamma_0(\varepsilon) = 1/\tau_{0i}(\varepsilon)$ of samples A and F, obtained by correction for the homogeneous broadening effect as described above, are shown in Figure 5. The clear energy dependence of Γ_0 is evident, where these two samples spectrally complement each other over a wide energy range with a partial overlap. This shows that the decay rates are sample independent and are influenced only by NC size (*i.e.*, the quantum confinement effect),[25] assuming that the NCs are spherical, and thus no shape effects are taken into consideration. In the same figure the radiative and total recombination rates for Si NCs extracted from variable optical mode density measurements are plotted.[22] The total recombination rates of Si NCs obtained here coincide with the reported radiative rate values from ref 22, suggesting near-unity IQE for the present ligand-passivated particles. Thereby we confirm the conjecture that the IQE in these ligand-passivated samples must be close to 100% in the full

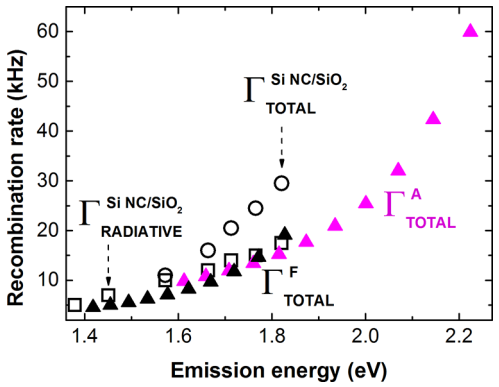

Figure 5. PL decay rates of samples A and F (triangles) obtained from spectrally resolved PL decay measurements at indicated energies. Corresponding PL decay times $\tau_{0i}(\varepsilon)$ were extracted by taking into account the homogeneous broadening effect. Previously reported radiative (rectangles) and total recombination rates (circles) of Si NCs embedded in SiO_2 are plotted with open symbols,[22] for comparison. The radiative rates of Si NCs in SiO_2 coincide with the measured total rates for both of the ligand-passivated Si NC samples.

range of emission energies. The fact that the radiative rate is the same for ligand- and SiO_2-passivated nanocrystals is not surprising, considering that the luminescence measured in both cases originates from the recombination inside the Si nanocrystal core, as evident from the typical microsecond lifetime (Figure 2, right) and the effect of core size on the peak position (Figure 1).

It was shown that the IQE for oxide-passivated silicon nanocrystals deviates from unity, suggesting the presence of a type (ii) nonradiative channel (comparable in strength with the radiative one) in that system.[22,37,43] In contrast, here we report IQE = 100% for Si NCs passivated with different ligand molecules in a full emission energy range, in which the nonradiative recombination channels of this type seem to be totally suppressed. A partial coverage of nanocrystal surface by oxygen molecules was confirmed here by FTIR measurements (Figure S2); hence a thick oxide shell is probably required to facilitate such a transition. Thus, the defect responsible for the nonradiative transition in the Si/SiO_2 system is most likely located inside the oxide shell. This can explain the relatively low rate of this transition since a carrier tunneling from the core would first be required for such a nonradiative recombination to occur, as illustrated in Figure 4b. So the similarities in the behavior of ligand- and oxide-passivated nanocrystals (Figure 5) originate from the recombination mechanism taking place in the silicon core; the differences in their optical performance (Figure 3) come from the passivating layer, more specifically from the associated defect sites, resulting in inferior IQE in the case of oxide-embedded nanocrystals.

CONCLUSIONS

In conclusion, spectrally resolved PL decay measurements were performed on various ligand-passivated Si NCs, and the PL decay parameters were extracted for different detection energies. A numerical method was suggested to apply mathematical size-selection and extract corresponding intrinsic size-dependent recombination rates and dispersion factors. It was found that the total decay rates, measured for specific emission energies, originate purely from the radiative recombination process. This is inferred from the extracted near-unity dispersion factors for size-selected ensembles supplying strong evidence of 100% internal luminescence efficiency of such Si NCs. The wavelength-independent near-unity IQE in ligand-passivated silicon nanocrystals makes this system superior to the oxide-embedded particles, where oxide-related defect states are known to substantially reduce the IQE in smaller nanocrystallites. We find this a remarkable observation, and thus further activities could be focused on increasing the fraction of bright nanocrystals, which would be beneficial for applications.

EXPERIMENTAL DETAILS

PL emission and absorption spectra as well as absolute QY were measured in a home-built apparatus based on the integrating sphere method.[44] It consists of a laser-driven xenon plasma white-light source (Energetic) with a wavelength-selecting monochromator for the excitation, 6 in. diameter integrating sphere (Labsphere), and thermoelectrically cooled CCD camera (Princeton Instruments) connected to a spectrometer for the detection. The excitation and detection signals were coupled to and from the integrating sphere by optical fibers. Before measurements the system response curve was evaluated using the same monochromatic light source calibrated with an optical power meter. It was done for the same spectrometer grating central wavelength positions as for actual measurements. Spectra for the sample and the reference solutions (toluene) were corrected for system response and subtracted from each other. Absolute QY is defined as the ratio between the number of absorbed and emitted photons, evaluated by integrating the resulting excitation and luminescence peak, respectively. The apparatus was tested by measuring Rhodamine 6G with a nominal QY value of ~95%,[45] yielding QY = 90−100% when excited within the Rhodamine 6G absorption band. For additional system validation, sample E was also tested in the University of Amsterdam, yielding QY = 47−55%, similar to the values reported here (*cf.* Figure 2, left). Another sample of ligand-passivated Si NCs with a measured here QY of 35−40% was independently tested in the commercial Hamamatsu Quantaurus-QY C9920-03 apparatus, resulting in a similar value of ~34%. Quantum yields were found to be independent of the excitation wavelength in accordance with the Kasha−Vavilov rule (*cf.* Figure S3).[46] In absorption measurements no wavelength selection was applied after the broadband excitation source. Transmitted white-light spectra through the integrating sphere with and without mounted sample solution were subtracted and normalized to the latter to get the relative absorption curve of the sample.

For PL decay measurements (spectral resolution $\Delta\lambda \approx 3$ nm), Si NC solutions in Suprasil quartz cuvettes were excited by a 405 nm laser beam, with the excitation power density of 2 W cm^{-2}. The excitation pulse width and frequency were

altered between 100−500 μs and 0.5−10 kHz, respectively, depending on the selected detection energy. An avalanche photodiode (Becker & Hickl, DPC-230) was used after a spectrometer (Andor Shamrock 500) in order to detect the emitted PL photons collected by a 10× objective lens (NA ≈ 0.25). Post binning was applied to the measured PL decay data to improve signal-to-noise ratio. For transmission electron microscope characterization sample solutions were drop-casted on ∼15 nm thick amorphous SiN membranes and imaged in a bright-field mode in a JEOL 2100 microscope using a 200 kV electron beam.

Conflict of Interest: The authors declare no competing financial interest.

Acknowledgment. Financial support from the Swedish Research Council (VR) through an individual contract and through a Linné grant (ADOPT) and from the Göran Gustafssons Foundation is gratefully acknowledged. The Veinot Research Group (J.G.C.V. and Z.Y.) thanks the Natural Science and Engineering Council of Canada for continued generous financial support. The authors would like to thank Bart van Dam, Chung Xuan, Nerijus Armakavicius, Anna Fucikova, Johnny Israelsson, and Rikard Friberg for help with quantum yield measurements.

Supporting Information Available: Photoluminescence decay curves of the sample A measured for the whole ensemble and detected at particular energies with extracted dispersion factors are shown in Figure S1 and the inset of Figure S1, respectively. FTIR spectra and QY as a function of excitation wavelength for different ligand-passivated Si NCs are presented in Figures S2 and S3, respectively. The Supporting Information is available free of charge on the ACS Publications website at DOI: 10.1021/acsnano.5b01717.

REFERENCES AND NOTES

1. Pavesi, L.; Lockwood, D. J. In *Silicon Photonics II*; Lockwood, D. J.; Pavesi, L., Eds.; Topics in Applied Physics; Springer: Berlin, 2011; Vol. 119.
2. Maier-Flaig, F.; Rinck, J.; Stephan, M.; Bocksrocker, T.; Bruns, M.; Kübel, C.; Powell, A. K.; Ozin, G. A.; Lemmer, U. Multicolor Silicon Light-Emitting Diodes (SiLEDs). *Nano Lett.* **2013**, *13*, 475–480.
3. Priolo, F.; Gregorkiewicz, T.; Galli, M.; Krauss, T. F. Silicon Nanostructures for Photonics and Photovoltaics. *Nat. Nanotechnol.* **2014**, *9*, 19–32.
4. Low, S. P.; Voelcker, N. H.; Canham, L. T.; Williams, K. A. The Biocompatibility of Porous Silicon in Tissues of the Eye. *Biomaterials* **2009**, *30*, 2873–2880.
5. Nishimura, H.; Ritchie, K.; Kasai, R. S.; Goto, M.; Morone, N.; Sugimura, H.; Tanaka, K.; Sase, I.; Yoshimura, A.; Nakano, Y.; *et al.* Biocompatible Fluorescent Silicon Nanocrystals for Single-Molecule Tracking and Fluorescence Imaging. *J. Cell Biol.* **2013**, *202*, 967–983.
6. Erogbogbo, F.; Yong, K.; Roy, I.; Hu, R.; Law, W.; Zhao, W.; Ding, H.; Wu, F.; Kumar, R.; Swihart, M. T.; *et al. In Vivo* Targeted Cancer Imaging, Sentinel Lymph Node Mapping and Multi-Channel Imaging with Biocompatible Silicon Nanocrystals. *ACS Nano* **2011**, *5*, 413–423.
7. Canham, L. T. Silicon Quantum Wire Array Fabrication by Electrochemical and Chemical Dissolution of Wafers. *Appl. Phys. Lett.* **1990**, *57*, 1046.
8. Lehmann, V.; Gösele, U. Porous Silicon Formation: A Quantum Wire Effect. *Appl. Phys. Lett.* **1991**, *58*, 856–858.
9. Kovalev, D.; Heckler, H.; Polisski, G.; Koch, F. Optical Properties of Si Nanocrystals. *Phys. Status Solidi B* **1999**, *215*, 871–932.
10. Cullis, A. G.; Canham, L. T.; Calcott, P. D. J. The Structural and Luminescence Properties of Porous Silicon. *J. Appl. Phys.* **1997**, *82*, 909–965.
11. Credo, G. M.; Mason, M. D.; Buratto, S. K. External Quantum Efficiency of Single Porous Silicon Nanoparticles. *Appl. Phys. Lett.* **1999**, *74*, 1978–1980.
12. Mangolini, L.; Jurbergs, D.; Rogojina, E.; Kortshagen, U. Plasma Synthesis and Liquid-Phase Surface Passivation of Brightly Luminescent Si Nanocrystals. *J. Lumin.* **2006**, *121*, 327–334.
13. Wilson, W. L.; Szajowski, P. F.; Brus, L. E. Quantum Confinement in Size-Selected, Surface-Oxidized Silicon Nanocrystals. *Science* **1993**, *262*, 1242–1244.
14. Vial, J.; Bsiesy, A.; Gaspard, F.; Hérino, R.; Ligeon, M.; Muller, F.; Romestain, R.; Macfarlane, R. Mechanisms of Visible-Light Emission from Electro-Oxidized Porous Silicon. *Phys. Rev. B* **1992**, *45*, 14171–14176.
15. Jurbergs, D.; Rogojina, E.; Mangolini, L.; Kortshagen, U. Silicon Nanocrystals with Ensemble Quantum Yields Exceeding 60%. *Appl. Phys. Lett.* **2006**, *88*, 233116–233118.
16. Mangolini, L.; Kortshagen, U. Plasma-Assisted Synthesis of Silicon Nanocrystal Inks. *Adv. Mater.* **2007**, *19*, 2513–2519.
17. Sychugov, I.; Juhasz, R.; Linnros, J.; Valenta, J. Luminescence Blinking of a Si Quantum Dot in a SiO_2 Shell. *Phys. Rev. B* **2005**, *71*, 115331–115335.
18. Skryshevsky, V. A.; Laugier, A.; Strikha, V. I.; Vikulov, V. A. Evaluation of Quantum Efficiency of Porous Silicon Photoluminescence. *Mater. Sci. Eng., B* **1996**, *40*, 54–57.
19. Sangghaleh, F.; Bruhn, B.; Sychugov, I.; Linnros, J. Optical Absorption Cross Section and Quantum Efficiency of a Single Silicon Quantum Dot. *Proc. SPIE* **2013**, *8766*, 876607–876612.
20. Walters, R.; Kalkman, J.; Polman, A.; Atwater, H.; de Dood, M. Photoluminescence Quantum Efficiency of Dense Silicon Nanocrystal Ensembles in SiO_2. *Phys. Rev. B* **2006**, *73*, 132302.
21. Kalkman, J.; Gersen, H.; Kuipers, L.; Polman, A. Excitation of Surface Plasmons at a SiO_2/Ag Interface by Silicon Quantum Dots: Experiment and Theory. *Phys. Rev. B* **2006**, *73*, 075317.
22. Miura, S.; Nakamura, T.; Fujii, M.; Inui, M.; Hayashi, S. Size Dependence of Photoluminescence Quantum Efficiency of Si Nanocrystals. *Phys. Rev. B* **2006**, *73*, 245333–245335.
23. Shu, Y.; Levine, B. G. Do Excited Silicon−Oxygen Double Bonds Emit Light? *J. Phys. Chem. C* **2014**, *118*, 7669–7677.
24. Skuja, L. Optically Active Oxygen-Deficiency-Related Centers in Amorphous Silicon Dioxide. *J. Non. Cryst. Solids* **1998**, *239*, 16–48.
25. Takagahara, T.; Takeda, K. Theory of the Quantum Confinement Effect on Excitons in Quantum Dots of Indirect-Gap Materials. *Phys. Rev. B* **1992**, *46*, 15578–15581.
26. Hessel, C. M.; Henderson, E. J.; Veinot, J. G. C. Hydrogen Silsesquioxane: A Molecular Precursor for Nanocrystalline Si−SiO_2 Composites and Freestanding Hydride-Surface-Terminated Silicon Nanoparticles. *Chem. Mater.* **2006**, *18*, 6139–6146.
27. Li, Z. F.; Swihart, M. T.; Ruckenstein, E. Luminescent Silicon Nanoparticles Capped by Conductive Polyaniline through the Self-Assembly Method. *Langmuir* **2004**, *20*, 1963–1971.
28. Pettigrew, K. A.; Liu, Q.; Power, P. P.; Kauzlarich, S. M. Solution Synthesis of Alkyl- and Alkyl/Alkoxy-Capped Silicon Nanoparticles *via* Oxidation of Mg_2Si. *Chem. Mater.* **2003**, *15*, 4005–4011.
29. Yang, Z.; Dobbie, A. R.; Cui, K.; Veinot, J. G. C. A Convenient Method for Preparing Alkyl-Functionalized Silicon Nanocubes. *J. Am. Chem. Soc.* **2012**, *134*, 13958–13961.
30. Yang, Z.; Gonzalez, C. M.; Purkait, T. K.; Iqbal, M.; Meldrum, A.; Veinot, J. G. C. Radical Initiator Driven Hydrosilylation on Silicon Nanocrystals. Manuscript in preparation.
31. Kelly, J. A.; Shukaliak, A. M.; Fleischauer, M. D.; Veinot, J. G. C. Size-Dependent Reactivity in Hydrosilylation of Silicon Nanocrystals. *J. Am. Chem. Soc.* **2011**, *133*, 9564–9571.
32. Pavesi, L.; Ceschini, M. Stretched-Exponential Decay of the Luminescence in Porous Silicon. *Phys. Rev. B* **1993**, *48*, 17625–17628.
33. Yang, Z.; De los Reyes, G. B.; Titova, L. V.; Sychugov, I.; Dasog, M.; Linnros, J.; Hegmann, F. A.; Veinot, J. G. C. Evolution of the Ultrafast Photoluminescence of Colloidal Silicon Nanocrystals with Changing Surface Chemistry. *ACS Photonics* **2015**, *2*, 595–605.
34. Hannah, D. C.; Yang, J.; Kramer, N. J.; Schatz, G. C.; Kortshagen, U. R.; Schaller, R. D. Ultrafast Photoluminescence in Quantum-Confined Silicon Nanocrystals Arises from an Amorphous Surface Layer. *ACS Photonics* **2014**, *1*, 960–967.

35. Poddubny, A. N.; Dohnalová, K. Direct Band Gap Silicon Quantum Dots Achieved *via* Electronegative Capping. *Phys. Rev. B* **2014**, *90*, 245439.
36. Linnros, J.; Lalic, N.; Galeckas, A.; Grivickas, V. Analysis of the Stretched Exponential Photoluminescence Decay from Nanometer-Sized Silicon Crystals in SiO_2. *J. Appl. Phys.* **1999**, *86*, 6128.
37. Sangghaleh, F.; Bruhn, B.; Schmidt, T.; Linnros, J. Exciton Lifetime Measurements on Single Silicon Quantum Dots. *Nanotechnology* **2013**, *24*, 225204.
38. Miller, J. B.; Van Sickle, A. R.; Anthony, R. J.; Kroll, D. M.; Kortshagen, U. R.; Hobbie, E. K. Ensemble Brightening and Enhanced Quantum Yield in Size-Purified Silicon Nanocrystals. *ACS Nano* **2012**, *6*, 7389–7396.
39. Sychugov, I.; Fucikova, A.; Pevere, F.; Yang, Z.; Veinot, J. G. C.; Linnros, J. Ultranarrow Luminescence Linewidth of Silicon Nanocrystals and Influence of Matrix. *ACS Photonics* **2014**, *1*, 998–1005.
40. Pevere, F.; Sychugov, I.; Sangghaleh, F.; Fucikova, A.; Linnros, J. Biexciton Emission as a Probe of Auger Recombination in Individual Silicon Nanocrystals. *J. Phys. Chem. C* **2015**, *119*, 7499–7505.
41. Hartel, A.; Gutsch, S.; Hiller, D.; Zacharias, M. Intrinsic Nonradiative Recombination in Ensembles of Silicon Nanocrystals. *Phys. Rev. B* **2013**, *87*, 035428.
42. Zacharias, M.; Hiller, D.; Hartel, A.; Gutsch, S. Defect Engineering of Si Nanocrystal Interfaces. *Phys. Status Solidi A* **2012**, *209*, 2449–2454.
43. Limpens, R.; Gregorkiewicz, T. Spectroscopic Investigations of Dark Si Nanocrystals in SiO_2 and Their Role in External Quantum Efficiency Quenching. *J. Appl. Phys.* **2013**, *114*, 074304–074310.
44. De Mello, J. C.; Wittmann, H. F.; Friend, R. H. An Improved Experimental Determination of External Photoluminescence Quantum Efficiency. *Adv. Mater.* **1997**, *9*, 230–232.
45. Kubin, R.; Fletcher, A. Fluorescence Quantum Yields of Some Rhodamine Dyes. *J. Lumin.* **1982**, *27*, 455–462.
46. Vavilov, S. I. Die Fluoreszenzausbeute von Farbstof Losungen Als Funktion Der Wellenlange Des Anregenden Lichtes. *Z. Phys.* **1927**, *42*, 311–318.